Energy Storage Through Magnesia Sulfatation in a Fluidized-Bed Reactor

C. Muller, G. Flamant
Institut de Science et de Génie des
Matériaux et Procédés,
C.N.R.S., B.P. no. 5,
Odeillo, 66120, Font-Romeu, France

Reversible gas-solid reactions have been proposed for heat storage or pumping applications by several investigators (Wenworth and Chen, 1976; Ervin, 1977).

The reaction $MgO + SO_3 \rightleftharpoons MgSO_4$ seems to be very attractive for high-temperature applications (Tmar et al., 1981). The endothermic reaction kinetics has been studied by Steinmetz et al. (1981): decomposition occurs at a temperature higher than 1,000°C and may be modeled by the shrinking-core concept. Research on the exothermic reaction has been developed by El Ghandour et al. (1983) using a fixed-bed reactor. They revealed that local overheating of the bed induces particle sintering. The overall reaction rate is limited by heat transfer. Notice that packed beds are not adapted to very fast reactive systems or to large particle volume variations (Mar, 1980). The literature on reversible chemical reactions for heat storage based on sulfates lacks heat transfer data on, for example, power to reactive volume ratio; this is because most previous experiments were run with small samples. We performed the reaction in a fluidized-bed reactor to measure these missing data.

Experimental Method

Set-up

The fluidized bed apparatus is shown schematically in Figure 1 and is described in detail by Muller (1985). The column is a stainless steel tube of 85 mm dia. and 250 mm height insulated with 50 mm thick alumina fiber. The gas distributor is a perforated plate with holes of 0.5 mm dia. and 0.5 mm pitch. The fluidizing gas is an N_2 (inert) and SO_3 (reactive) mixture; it is preheated in a heat exchanger before passing through the bed of MgO particles. SO_3 is produced from the liquid evaporation: its mass flow rate is obtained from a flowmeter conjugate to the measurement of the evaporator weight decrease with time. An annular electric heating element circles the reactor wall in order to regulate the initial bed temperature.

The bed temperature is measured with five bare thermocouples; 20 temperature probes control the overall loop. The gas pressure drop is determined using a differential pressure gauge whose signal is filtered to be related to the mean solid conversion. A calorimeter has been designed to perform the reaction under isothermic conditions. It is composed of two concentric tubes forming an annular water-drained zone. The water temperature increase is measured by two electronic transducers to within ±0.01°C.

Technique and procedure

Heat and mass balances over the reactor are based on continuous measurement of oxide conversion X_o, SO_3 flow rate F_{SO_3}, bed temperature T_b, and evolved power P.

The solid conversion continuous measurement is obtained using an original method developed by Muller and Flamant (1986). The conversion is deduced from pressure drop measurements. The relation is:

$$X = \frac{1}{\delta_m} \frac{|\Delta P - \Delta P_o|}{\Delta P_o} \quad \text{with} \quad \Delta P = \frac{m \cdot g}{A_b} \tag{1}$$

where ΔP_o and ΔP are the pressure drops at time $t = 0$ and t.

A corrective factor, F_c, defined as the ratio of the theoretical pressure drop, Eq. 1, to the actual drop, accounts for the dead zones near the distributor plate. F_c is found to range from 1.01 to 1.08.

In order to obtain isothermic conditions and to measure the evolved power P, the calorimeter is immersed in the bed. The water flow rate and the water temperature increase are measured to calculate the evolved power. The bed temperature is changed by moving the device vertically. The bed-to-wall heat transfer coefficient, h_b, may be deduced easily from experimental data (Bock, 1981; Osman et al., 1982).

The three-phase experimental procedure is as follows:

1. The magnesia bed is fluidized with nitrogen and preheated up to the initial bed temperature using the electric heater.

*Correspondence concerning this paper should be addressed to G. Flamant.

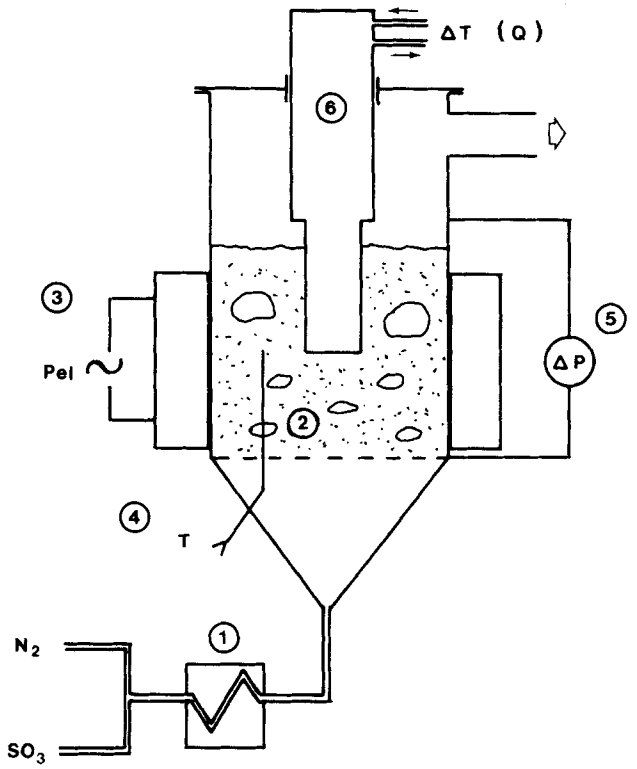

Figure 1. Experimental set-up.

1. Heat exchanger
2. Bed, MgO particles
3. Heating element
4. Temperature probe
5. Pressure gauge
6. Calorimeter

2. The sulfur trioxide is introduced in the reactor at time $t = t_1$. During the reaction phase, $\Delta P(t)$, $T_b(t)$, and $P(t)$ are recorded and stored on a magnetic tape.

3. The reaction is stopped at $t = t_2$ when a large decrease of the reaction rate is observed, and finally the bed is cooled down.

The experimental study main parameters are:

- Initial bed temperature, T_b^o
- Mean particle diameter, d
- Magnesia density (or internal porosity) ρ_o (or ξ_o),
- SO_3 mass flow rate, F_{SO_3}

Their variation ranges are summarized in Table 1.

Results and Discussion

First, in order to emphasize the good solid mixing and heat transfer properties of the bed even for fast exothermic reactions, data from the five bed-immersed thermocouples are compared to the mean bed temperature for each experiment. The measured mean deviation is 4°C up to $T_b = 1{,}000$°C.

Table 1. Experimental Parameters, Variation Range

Particle dia., 10^{-3} m	0.1–1.2
Solid density, 10^3 kg · m^{-3}	0.5–3.6
Initial MgO weight, 10^{-3} kg	18–435
Initial bed temp., °C	80–790
SO_3 mass flow rate, 10^{-3} kg · s^{-1}	0.07–0.8
Fluidization number U/U_{mf}	2–6

Adiabatic runs

Several significant results are listed in Table 2. Runs number 10 and 4 show that the reaction may occur at temperatures as low as 80°C. No significant variation of the reaction rate is observed in the range 80–790°C because the SO_3 conversion is always complete. X_o vs. t and T vs. t curves related to run 10 are shown in Figure 2. ΔP vs. t is drawn to illustrate the solid conversion measurement method. In Figure 2, the X_o vs. t curve is calculated assuming $F_c = 1$ (ideal case). The real solid conversion vs. time takes the final solid conversion into account: the comparison between the results of the pressure drop measurement and of a thermal decomposition method leads to the correction factor F_c. The actual solid conversion is given in Figure 3 for $F_c = 1.07$ ($\delta_m = 1.98$).

The maximum operating temperature T^* depends on thermodynamics and on experimental conditions (particularly inert ratio, RI, and total pressure, P_R). Runs 14 and 15 indicate $T^* = 1{,}020 \pm 5$°C when $RI = 2$ and $P_R = 0.85$ atm.

Runs 1, 4, and 3 point out the influence of the particle mean diameter on MgO final conversion X_f, which decreases when the mean diameter d increases; for example $X_f = 0.82$ and 0.40 for $d = 375$ and 1,000 μm, respectively. Typical X_o vs. t results are shown in Figure 3 for $d = 375$ and 750 μm (runs 10 and 14). A two-step conversion occurs with the largest particles: a constant rate period and a decreasing rate period. The apparent reaction rate variation between both steps is larger than one order of magnitude and during step 2 the SO_3 conversion is less than one. Let us define X_f' as the solid conversion at the transition between both steps, and X_f as the final conversion. Figure 4 indicates a large decrease of X_f' and X_f with particle diameter. Therefore, for energy storage application the reaction progress has to be limited to the fast reaction period if small particles are used.

The dependence of the oxide final conversion, X_f, on the magnesia particle internal porosity ξ_o is plotted in Figure 5. Data

Table 2. Various Experimental Results, Adiabatic Runs

Run	d 10^{-6} m	ρ_o kg · m^{-3}	ξ_o	m_o 10^{-3} kg	F_{SO_3} 10^{-3} kg · s^{-1}	RI	X_f	T_b^o · °C	T_b^{max} · °C
10	250–500	500	0.86	72.7	0.33	2	0.95	80	620
4	250–500	500	0.86	83.5	0.12	3.5	0.82	790	940
1	125–1,000	500	0.86	145.5	0.29	2	0.66	530	780
13	1,000–1,200	500	0.86	145.5	—	—	0.40	145	600
14	500–1,000	500	0.86	100	0.57	2	0.74	730	1,025
15	500–1,000	500	0.86	145.5	0.33	2.5	0.85	760	1,020
22	50–100	1,350	0.62	145.5	0.07	4	0.40	360	600
24	100–160	1,900	0.47	145.5	0.13	4	0.20	330	450
11	500–1,000	500	0.86	36.4	0.81	2.2	0.74	280	900

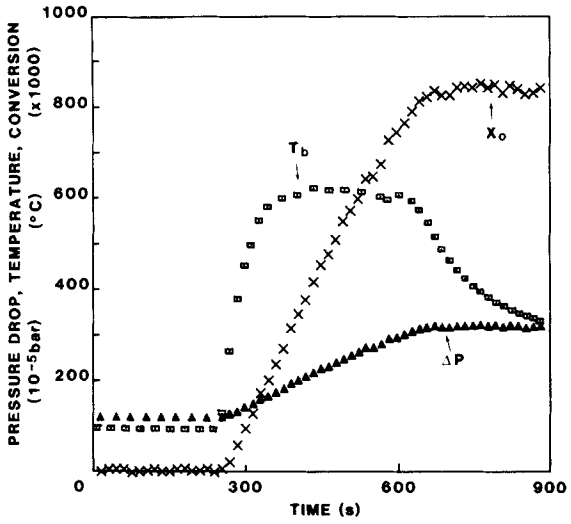

Figure 2. Adiabatic run 10.

Δ Pressure drop; X solid conversion; O bed temperature
Correction coefficient not used; $F_c = 1$

related to points A, B, and C are listed in Table 2: runs 10, 22, 24, respectively. Changing the internal porosity from 0.86 to 0.47 decreases the conversion from 0.95 to 0.20. A very simple approach may be formulated to evaluate the solid final conversion as a function of magnesia porosity. The sulfation of magnesium oxide is attended with a large increase in molecular volume, from 11.1 to 44.4 $cm^3 \cdot mol^{-1}$. Let us assume that the particle volume v_p is constant; then the internal porosity decreases during the reaction because of the solid molecular volume increase. Thus the oxide final conversion corresponds to the value $\xi_s = 0$. Let us introduce ξ_o^{min} (or ρ_o^{min}), the initial internal porosity minimum value required to reach $X_f = 1$. ξ_o^{min} is defined as:

$$\xi_o^{min} = 1 - \frac{M_o/\rho_o^c}{M_s/\rho_s^c} \tag{2}$$

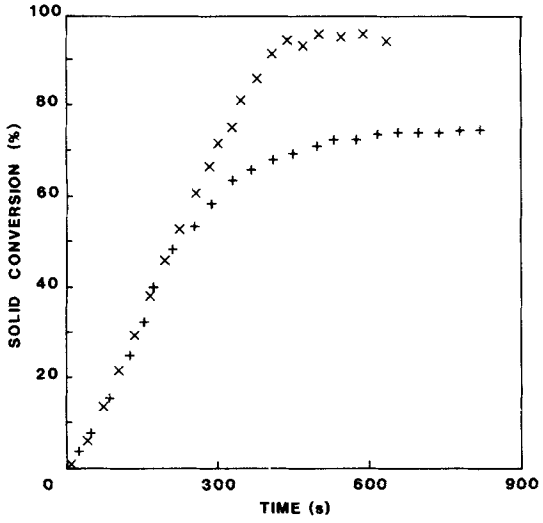

Figure 3. Solid conversion vs. time.

X, $\bar{d} = 375$ μm (run 10)
+, $\bar{d} = 750$ μm (run 14)

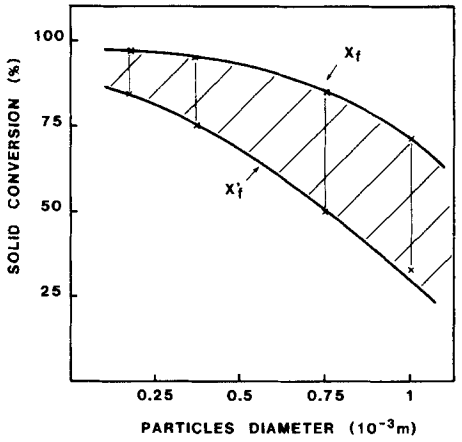

Figure 4. Final solid conversion X_f and intermediate solid conversion X'_f vs. mean particle diameter.

in which ρ_o^c and ρ_s^c are respectively the oxide and the sulfate crystal densities ($\xi_o = 0$).

Because of the previous assumption (v_p = constant), the conversion X_f may be predicted as:

$$X_f = 1 \quad \text{if } \xi_o^{min} < 0 < 1$$

$$X_f = \frac{\xi_o/(1-\xi_o)}{\xi_o^{min}/(1-\xi_o^{min})} \quad \text{if } 0 < \theta_o < \xi_o^{min} \tag{3}$$

Previous relations are plotted in figure 5, curve 2. A satisfying agreement is observed between predicted and experimental data.

A large SO_3 flow rate was imposed for run 11 in order to operate without mass transfer limitation. The mass balance over the reactor indicates a complete SO_3 conversion during the first reaction period and an apparent reaction rate of about 5 kg $SO_3 \cdot m^{-3} \cdot s^{-1}$.

Isothermic runs

The experimental procedure main problem is the determination of the proper heat exchange area between the bed and the calorimeter for a selected working temperature. Temperature

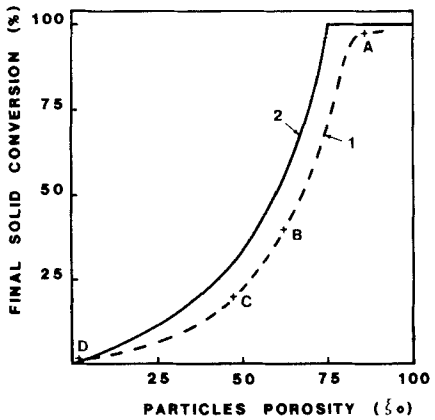

Figure 5. Final solid conversion vs. internal particles porosity

1. Experimental; 2. Theoretical

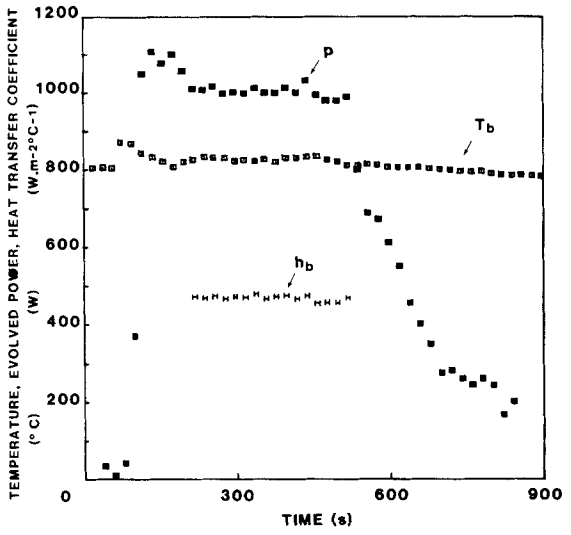

Figure 6. Isothermic run.

T_b, Bed temperature; p, evolved power; h_b, heat transfer coefficient
$d = 280\ \mu m$; $\xi_o = 0.86$; $m_o = 104$ g; $F_{SO_3} = 0.31$; $RI = 2.2$

fluctuations are observed when the calorimeter is moved vertically. Results for 800°C mean bed temperature are shown in Figure 6. The bed temperature, the evolved power, and the heat transfer coefficient are plotted vs. time. During the reacting period (about 7 min) the power exchanged between the bed and the calorimeter reaches 1 kW, and the heat transfer coefficient is 470 W · m^{-2} · C^{-1} for 280 μm mean dia. particles. No significant variation of h_b is observed during the experiment. The overall heat balance over the reactor gives the following results:

Evolved power, 15 MW · m^{-3} (related to the bed volume)

Energy-to-volume ratio, 500 kWh · m^{-3} (bed voidage: 0.5)

Concluding remarks

For heat storage or heat pumping applications, the reactive system (reactants plus reactor) has to provide a high value of the power-to-volume ratio and it must be flexible. Experimental data suggest the following criteria:

- Particles: $d < 300\ \mu m$; $\xi_o \geq 0.75$
- Temperature: 100°C $< T_b <$ 900°C
- Solid conversion: $X_o < X'_f$

The consequence of this selection is a very simple control method base on SO_3 mass flow rate because the overall reaction rate is controlled by SO_3 flow up to 5 kg · m^{-3} · s^{-1}.

A simplified model for predicting the reactor unsteady behavior under the previous limited conditions is discussed next.

Theory

According to experimental data, magnesia sulfatation is a fast transformation and the progress of reaction is limited by SO_3 flow rate up to a large value of the power-to-bed volume ratio. Since the reaction is mass-transfer controlled and the reactor is well stirred, the reactor simulation during the first period (constant rate regime) is based on the following assumptions:

1. The bed is homogeneous, the gas and the solid are perfectly mixed
2. The pressure is constant inside the reactor
3. The solid and the gas temperatures are equal and the bed temperature is uniform
4. The gas weight is low compared to the solid weight
5. No parallel reaction occurs
6. The SO_3 conversion = 1
7. No chemical or thermodynamical limitations are taken into account

The homogeneous approximation validity is discussed by Beek (1972). The criteria are respected in this study (Muller, 1985).

Model formulation

In order to describe the bed temperature and the solid conversion variation with time during the experiments, the three periods experimental procedure is respected.

Mass Balance. The mass balance equation related to the oxide is:

$$X_o(t) = \frac{t - t_1}{\tau} \quad \text{for } t_1 < t < t_2 \tag{4}$$

Heat balance. The equation is, assuming $T_R = T_b = T$:

$$q = \left[\Delta H_r(T)\,\frac{M_s}{M_{SO_3}}\,F^i_{SO_3}X_{SO_3}\right] + \left[F^i_{SO_3}C_{pSO_3}(T - T^i_g) + F_I C_{pI}(T - T^i_I)\right] + \left[m_o(t)C_{po} + m_s(t)C_{pS} + m_R C_R\right]\frac{dT}{dt} \tag{5}$$

in which $\Delta H_r(T)$ is the reaction enthalpy per kilogram of $MgSO_4$.

The heat from surroundings and heating elements is defined by:

$$q = p_{el} - K(T - T_a) \tag{6}$$

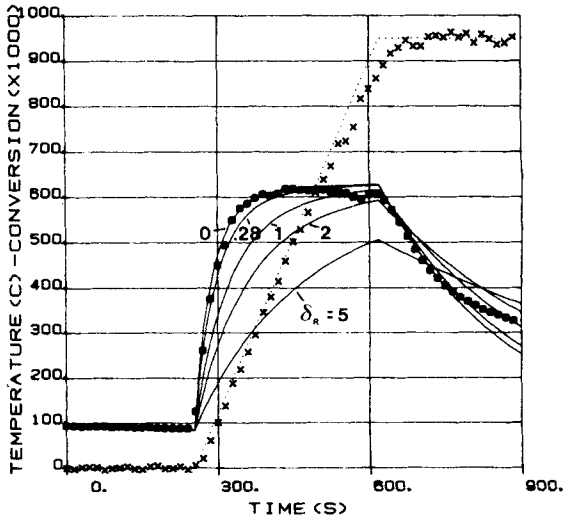

Figure 7. Comparison of experimental results, run 10, with simplified model.

Bed temperature as a function of reactor thermal inertia parameter δ_R
$K_1 = K_3 = 0.5$ W · C^{-1}; $K_2 = 1.4$ W · C^{-1}

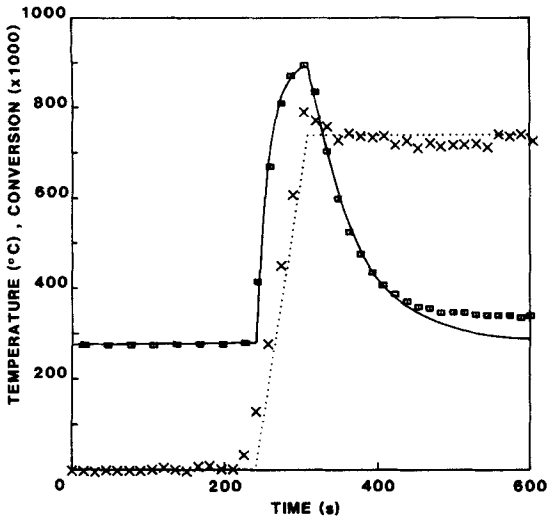

Figure 8. Experimental and theoretical data for run 11.
Bed temperature and solid conversion vs. time. Theoretical results
— bed temperature; · · · · · · solid conversion
$\delta_R = 0.3$; $K_1 = K_3 = 0.92$ W · C^{-1}; $K_2 = 2$ W · C^{-1}

Introducing dimensionless groups δ_R, δ_X, δ_m, Eq. 11 becomes for $t_1 < t < t_2$:

$$m_o C_{pO}\left(1 + \delta_R + \delta_X \frac{t - t_1}{\tau}\right)\frac{dT}{dt} + (F^i_{SO_3} C_{pSO_3} + F_I C_{pI} + K)T = -\Delta H_r(\delta_m^{-1} + 1)F^i_{SO_3} + (F^i_{SO_3} C_{pSO_3} + F_I C_{pI})T^i_g + P_{el} + KT_a \quad (7)$$

Results and discussion

Figure 7 shows the comparison between computed and experimental T and X_o vs. t profiles related to run 10. Theoretical curves (solid lines) are calculated for δ_R ranging from 0 to 5. A good agreement is observed for a small value of the reactor thermal inertia, $\delta_R = 0.15$. In general, the model predictions are more sensitive to the heat loss parameter K than to the thermal inertia parameter δ_R. Therefore the measured temperature profile is calculated for a value of K, then fitted by varying δ_R. Another result is plotted in Figure 8 related to run 11. The fast temperature rise and decrease (17°C · s^{-1}) is well predicted by the model.

Notation

A_b = cross-sectional area of fluidized bed column
C_{pi} = specific heat at constant pressure per kg of component i
C_R = specific heat of reactor wall
F_c = correction coefficient
F_i = mass flow rate of component i
g = acceleration of gravity
h = heat transfer coefficient
K = heat loss coefficient between reactor and surroundings
m = bed weight
M_i = molar weight of component i
P = evolved power measured with calorimeter
P_{el} = electric power absorbed by system
q = heat flux
RI = inert gas ratio, $(F_I/M_I)/F_{SO_3}/M_{SO_3}$)
T_b = bed temperature
T^* = equilibrium temperature
t = time
U = fluidization gas velocity
X_i = conversion of component i

Greek letters

ΔP = pressure drop
ΔH_r = reaction enthalpy
$\delta_m = (M_g - M_O)/M_O$
$\delta_R = (M_R C_R)/(m_O C_{pO})$
$\delta_X = (C_{pS} M_S - C_{pO} M_O)/(C_{pO} M_O)$
ξ = porosity
ρ = density
τ = stoichiometric time $\tau = (m_o/M_O)/F_{SO_3}/M_{SO_3})$

Subscripts

a = ambient
b = bed
el = electric
f = final
I = inert gas
o = oxide
p = product
R = reactor
r = reaction or reactant
S = sulfate
SO_3 = related to sulfur trioxide
W = wall

Superscripts

C = crystal
i = inlet
o = initial

Literature Cited

Beek, W. J., "Mass Transfer in Fluidized Bed," *Fluidization,* Davidson and Harrison, ed., Academic Press, London, 431 (1971).
Bock, H. J., "Dimensioning of Vertical Heat Transfer Surfaces in Gas-Solid Fluidized Beds," *Ger. Chem. Eng.*, **4,** 356 (1981).
El Ghandour, N., R. Valls, and M. Ducarroir, "Stockage par Reactions Renversables: Restitution de l'Énergie Thermique par Synthèse de Sulfate et Influence du Cyclage," *Bull. Soc. Chim. Fr.*, p. 133 (1983).
Ervin, G., "Solar Heat Storage Using Chemical Reactions," *J. Solid State Chem.*, **22,** 51 (1977).
Mar, R., "Materials Science Issues Encountered During the Development of Thermochemical Concepts," *Solar Material Science,* L. E. Murr, ed., Academic Press, 459 (1980).
Muller, C., "Stockage Chimique de l'Énergie à Haute Température. Etude de la Phase de Restitution pour le Système MgO, SO_3/$MgSO_3$ en Lit Fluidisé," Thèse de Docteur Ingénieur, Université de Perpignan, France (1985).
Muller, C., and G. Flamant, "Suivi d'une Réaction Gaz-Solide en Lit Fluidisé par Mesure de la Perte de Charge," *Entropie,* **127,** 37 (1986).
Osman, M. I., S. N. Upadhya, and S. C. Saxena, "Heat Transfer Investigation for Bed and Freeboard Vertical U-tubes in Fluidized Bed at Moderated Temperature," *Energy,* 7(5), 465 (1982).
Steinmetz, D., M. Ducarroir, H. Romero-Paredes, and M. Rivot, "Cinétique de Décomposition du Sulfate de Magnésium en Vue du Stockage de l'Énergie Solaire," *Entropie,* **102,** 18 (1981).
Tmar, M., C. Bernard, M. Ducarroir, "Local Storage of Solar Energy by Reversible Reaction with Sulfates," *Solar Energy,* **26,** 529 (1981).
Wenworth, N. E., and E. Chen, "Simple Thermal Decomposition Reactions for Storage of Solar Thermal Energy," *Solar Energy,* **26,** 205 (1976).

Manuscript received Aug. 26, 1986, and revision received Sept. 22, 1987.